Energy Conversion and Management 179 (2019) 30–45

Contents lists available at ScienceDirect

Energy Conversion and Management

journal homepage: www.elsevier.com/locate/enconman

Thermal-hydraulic performance and entropy generation analysis of a parabolic trough receiver with conical strip inserts

Peng Liu, Nianben Zheng, Zhichun Liu, Wei Liu*

School of Energy and Power Engineering, Huazhong University of Science and Technology, Wuhan 430074, China

ARTICLE INFO

Keywords:
Parabolic trough receiver
Conical strip inserts
Thermal-hydraulic performance
Heat loss
Entropy analysis

ABSTRACT

This paper presents a numerical study on the thermal-hydraulic and thermodynamic performance of a parabolic trough receiver with conical strip inserts. The effects of geometric parameters including central angle, hollow diameter, and pitch ratio on the performances are determined. The mass flow rate is found to vary in the range of 0.57–11.40 kg/s, with the corresponding Reynolds number ranging from 5000 to 791,000, which depends on the fluid inlet temperature. In the present study, four fluid inlet temperatures (400, 500, 600 and 650 K) are applied, and it is found that the heat transfer is effectively enhanced by the conical strip inserts, with the Nusselt number being enhanced 45–203%. Consequently, the temperature of the absorber tube and the heat loss are apparently reduced and the maximum reduction in heat loss is 82.1%. However, considerable increase in pressure loss penalty is also caused by the inserts, with the friction factor being 6.17–17.44 times that of the smooth parabolic trough receiver. Thus, the overall thermal-hydraulic performance (performance evaluation criteria) is ranged in 0.70–1.33, and the thermal efficiency is enhanced by 0.02–5.04%. In addition, Entropy and exergy analysis is carried out and it is found that for every given value of geometric parameters and fluid inlet temperature, there is a Reynolds number or mass flow rate below which the entropy generation rate is lower than that of the smooth parabolic trough receiver. The maximum reduction in entropy generation rate achieved in this study is 74.2% and the maximum enhancement in the exergetic efficiency is approximately 5.7%.

1. Introduction

Solar energy is a widely distributed renewable and clean energy source, and thus, its utilization is one of the most significant ways for solving problems such as global warming, fossil fuel depletion, and increasing energy demand [1]. Presently, the parabolic trough collector (PTC) plant is one of the most prevalent commercial techniques for solar energy utilization [2]. As the key component of a PTC plant, the parabolic trough receiver (PTR) accounts for approximately 30% of the system cost, and fulfills a very important role because the reliability, energy-collecting efficiency, and economic efficiency of PTC are profoundly dependent on its performance [3]. Therefore, it plays a significant role in improving PTR performance.

The PTR can effectively produce heat at high temperatures, with the temperature of the heat transfer fluid (HTF) up to 400 °C [4]; the temperature of the absorber tube can be even higher. Moreover, a high circumferential temperature gradient is produced in the tube because of the highly non-uniform heat flux generated from the concentrated solar radiation. Furthermore, in some cases, higher concentration ratios are applied to reduce the number of drives and connections to reduce cost, which will further lead to a higher circumferential temperature gradient and temperature in the absorber tube [5]. Consequently, these severe operation conditions of a high circumferential temperature gradient and temperature in the absorber tube may have several adverse effects on the performance and reliability of the PTR. On the one hand, an excessively high temperature can lead to degradation of the HTF and significantly increase the heat loss, thus reducing the energy-collecting efficiency of the PTR. On the other hand, the high circumferential temperature gradient can cause a large thermal stress in the absorber tube, which may bend the tube and even break the glass cover, thus reducing the life time of the PTR. Heat transfer enhancement techniques are an effective method of overcoming these problems. Bellos [6] reviewed and compared the applications of nanofluids and turbulators for thermal enhancement in PTR. Fuqiang [7] reviewed the progress in techniques with PTC system. It is found that nanofluids and turbulators are the most usual thermal enhancement techniques for PTR.

Nanofluids, which have great potential to enhance the thermal performance in PTR [8], have drawn extensive research attention. Until now, various nanofluids have been proposed and investigated.

* Corresponding author.
E-mail address: w_liu@hust.edu.cn (W. Liu).

https://doi.org/10.1016/j.enconman.2018.10.057
Received 3 July 2018; Received in revised form 12 October 2018; Accepted 17 October 2018
Available online 25 October 2018
0196-8904/

Nomenclature

c_p	specific heat capacity, J/(kg·K)
d	hollow diameter of inserts, mm
DNI	direct normal irradiance, W/m^2
f	friction factor
f_0	friction factor of a plain tube
h	heat transfer coefficient, W/m^2 K
h_w	heat transfer coefficient of glass cover outer wall, W/(m^2 K)
k	turbulent kinetic energy, m^2/s^2
L	the full length of PTR, mm
Nu	Nusselt number
Nu_0	Nusselt number of a plain tube
Nu_{cir}	the circumferentially-average Nusselt number
$N_{S,en}$	entropy generation ratio
P	pressure, Pa
p	the pitch of conical strip, mm
p^*	the pitch ratio
PEC	performance evaluation criteria
q	heat flux per unit area, W/m^2
Re	Reynolds number
S_{gen}	total entropy generation rate, W/(m^3 K)
S'_{gen}	entropy generation rate per unit volume, W/(m^3 K)
$S_{gen}{}^F$	entropy generation rate from the fluid friction irreversibility, W/(m^3 K)
S'^F_{gen}	the fluid friction irreversibility per unit volume, W/(m^3 K)
$S_{gen}{}^H$	entropy generation rate from the heat transfer irreversibility, W/(m^3 K)
S'^H_{gen}	the heat transfer irreversibility per unit volume, W/(m^3 K)
T	temperature, K
T_{cir}	the circumferentially-average temperature, K
T_f	fluid bulk temperature, K
T_{inlet}	mass average temperature of the fluid in inlet, K
T_{max}	maximum temperature of absorber tube inner wall, K
T_w	temperature of absorber tube inner wall, K
u	fluid velocity, m/s
u_{inlet}	the average velocity at the inlet of absorber tube, m/s
V_w	wind velocity, m/s
ΔP	the pressure drop between the inlet and outlet of the absorber tube, Pa
ΔT	the difference between the absorber tube maximum and minimum temperature, K

Greek symbols

α	thermal diffusivity, m^2/s
β	central angle of inserts, (°)
δ	The space between the conical strips and absorber tube inner wall, mm
ξ	emissivity
φ_r	collector rim angle, (°)
θ	receiver angle, (°)
λ	fluid thermal conductivity, W/m K
μ	viscosity, Pa s
ρ	density, kg/m^3

Mwesigye et al. conducted studies on the PTR with silver-Therminol VP-1 [9] and Cu-Therminol®VP-1 [10] as HTF. They found that the silver-Therminol VP-1 and Cu-Therminol®VP-1 can obtain 13.9% and 12.5% increases in thermal efficiency, respectively. Kasaeian et al. [11] proposed that an average 11% increase in global efficiency of PTR was achieved by suing carbon nanotube nanofluid. Bellos et al. [12] studied oil- and molten salt-based nanofluids for PTRs, and found that oil-based nanofluid performs better than molten salt-based nanofluid. Toghyani et al. [13] investigated the nanofluid base PTC in an integrated Rankine cycle and found that the nanofluid can increase the overall exergy efficiency. Coccia et al. [14] reported an adoption of nanofluids in low-enthalpy PTCs. Subramani et al. [15] reported a research of PTCs using TiO_2 nanofluids, which achieved an 8.66% increase in collector efficiency and approximately 23% improvement in the heat transfer coefficient. However, because of their several drawbacks such as high production costs, instability, and agglomeration, the nanofluid techniques are still under lab-scale research and not ready for extensive industrial application [16]. Adding turbulators to the absorber tube (or using configurated tubes), are the most prevalent and applicable passive techniques for heat transfer enhancement, because they do not require any external power and are easy to manufacture and install. Various configurations of absorber tube wall including different finned tubes (pin-finned tube [17], internally finned tube [18], helically finned tube [19], and longitudinally finned tube [20]), internally dimpled tube [21], corrugated tube [22], asymmetric outward convex corrugated tube [23], and sinusoidal tube [24], have been investigated and reported to improve the PTR performance by disturbing the fluid near the tube wall and obtaining a thinner thermal boundary layer to enhance the heat transfer. Gong et al. [17] achieved 12% enhancement in overall heat transfer performance by using pin fin arrays insert. Bellos et al. conducted comprehensive studies on PTR with internally finned tube [18] and longitudinal finned tube [20]. Muñoz [19] performed a numerical study on effects of helically finned tube on performance of PTR. Performance of dimpled tubes in PTR under non-uniform and uniform heat flux were numerically investigated by Huang et al. [21], and it was found that the dimpled receiver tube under non-uniform heat flux can obtain a better performance. Fuqiang et al. evaluated the thermal performance of PTR with corrugated tube [22] and asymmetric outward convex corrugated tube [23]. Bitam et al. [24] proposed a novel sinusoidal tube in PTR and numerically studied its performance. Similarly, many types of inserts such as tape inserts (wall-detached twisted tape [25], helical screw-tape [26], and wavy-tape [27]), metal foams [28], porous media [29], porous disc [30], and perforated plate inserts [31] have been applied and examined for heat transfer enhancement in the absorber tube. Some of them can form longitudinal vortex flows. For example, Mwesigye et al. [25] examined the heat transfer and entropy generation performance of tube with wall-detached twisted tape in PTR. Song et al. [26] proposed that the helical screw-tape insert can greatly reduce the heat loss, peak temperature and temperature gradient of the PTR. Some of them can enhance the thermal conductivity thus improve the collector efficiency, such as porous media [29]. Others can direct fluid to flush the tube wall. For instance, both the porous disc [30] and perforated plate inserts [31] obtain effectively enhancement in heat transfer. Because of the non-uniform heat flux condition, a very high temperature is generated in the heat-concentrated zones. Thus, these areas have greater requirements for heat transfer enhancement than other areas. For this purpose, Wang et al. [28] fitted metal foams in the low part of the absorber tube, where a high concentrated heat flux was situated, and found the thermal performance to apparently improve. Cheng et al. [32] found that unilateral longitudinal vortex generators can obtain an advanced performance. Zhu et al. [27] have recently reported a wavy-tape inserts, which can significantly enhance the localized heat transfer on the heat concentrated zones. They found that the heat transfer performance was significantly improved with 261–310% enhancement in the global-average Nusselt number.

Recently, Liu et al. conducted an optimization of heat transfer in a circular tube based on exergy destruction minimization and found that the multiple longitudinal swirl flow is the optimal flow field for heat transfer [33]. In addition, they proposed a conical strip inserts to realize the optimal flow field for heat transfer enhancement in a circular tube [34]. It is found that the conical strips can guide the cold fluid to flush the tube wall and lead to a high local heat transfer coefficient in this area. This insert is expected to effectively reduce the absorber tube temperatures and improve PTR performance. However, none of the studies have used conical strip inserts for the PTR. Therefore, in the present study, a conical strip insert is introduced to improve the PTR performance. In addition, the effects of these inserts on the thermal-hydraulic performance of the PTR are numerically investigated. Furthermore, analyses of heat loss and entropy generation are conducted.

2. Physical model

A schematic of a PTR with conical strip inserts is presented in Fig. 1(a) and (b). The conical strips are carved up from a hollow circular truncated cone with a hollow diameter (d) and attached to a circular rod of diameter 6 mm. In addition, each conical strip has a central angle (β), the pitch of the strips is defined by the space between two conical strips (p). The space between the conical strips and absorber tube inner wall (δ) is 3 mm. An LS2 PTC from CAMDA New Energy Equipment Co., Ltd is used in the present study. The receiver parameters are as follows: length (L) of the PTC is 7.8 m, the inner (d_{ri}) and outer (d_{ro}) diameters of the absorber tube are 66 and 70 mm, respectively, and the inner (d_{gi}) and outer (d_{go}) diameters of the glass cover are 109 and 115 mm, respectively. In addition, the effects of different pitch ratios ($p^* = p/d_{ri}$ = 0.5, 1, 1.5, and 2), hollow diameters (d = 20, 30, 40, 50 mm), and central angles (β = 40°, 50°, 60°, 70°, 80°, 90°) on the heat transfer and thermodynamic performance of PTRs are investigated.

To save computational resources and taking into account the symmetry of the geometric model, a periodic module with a length of only one pitch of the PTR and only half of the periodic module with a symmetric boundary condition is considered in this analysis. The calculation domain used in this study is displayed in Fig. 1(c).

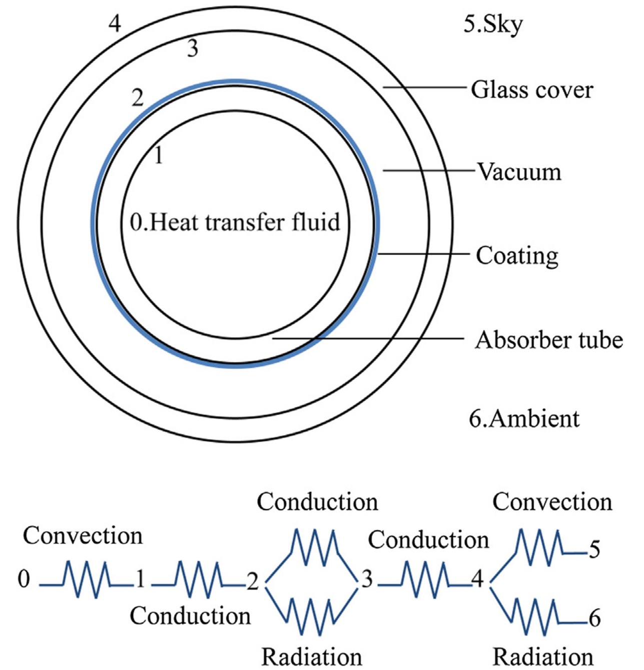

Fig. 2. Cross-section of the PTR and the corresponding thermal network.

3. Numerical model

In this section, the governing equations are not described in detail instead referred to the literature. The description of numerical model is focused on boundary conditions and solution procedure. Parameter definitions are also introduced. Moreover, Mesh generation and independence test are performed and described in this section.

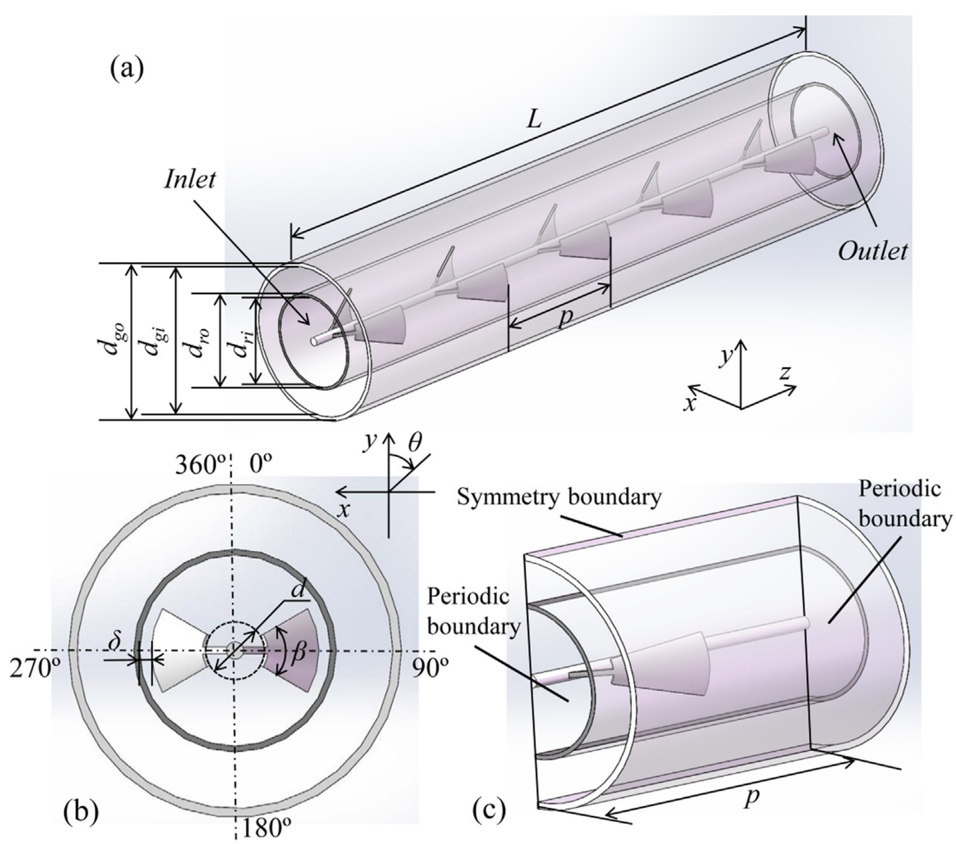

Fig. 1. (a) Schematic of the PTR with conical strip inserts, (b) cross-section of the enhanced PTR, (c) periodic calculation domain.

Table 1
Fourier formulas of heat flux distribution.

θ range	$q = a_0 + a_1\cos(\omega\theta) + b_1\sin(\omega\theta) + a_2\cos(2\omega\theta) + b_2\sin(2\omega\theta)$					
	ω	a_0	a_1	b_1	a_2	b_2
$0^\circ \le \theta < 41.6^\circ$	0	680	0	0	0	0
$41.6^\circ \le \theta < 88.6^\circ$	0.0588	35,120	25,470	−24,250	1464	−671
$88.6^\circ \le \theta \le 180^\circ$	0.0312	56,160	−11290	10,510	−4039	−1582

Table 2
Properties of HTF (Syltherm-800).

Properties	$a + bT + cT^2 + dT^3 + eT^4$				
	a	b	c	d	e
μ, Pa s	8.4866×10^{-2}	-5.5412×10^{-4}	1.3882×10^{-6}	-1.5660×10^{-9}	6.672×10^{-13}
λ, W m^{-1} K^{-1}	1.9002×10^{-1}	-1.8752×10^{-4}	-5.7534×10^{-10}	–	–
c_p, J kg^{-1} K^{-1}	1.1078×10^{3}	1.7080	–	–	–
ρ, kg m^{-3}	1.1057×10^{3}	-4.1535×10^{-1}	-6.0616×10^{-4}	–	–

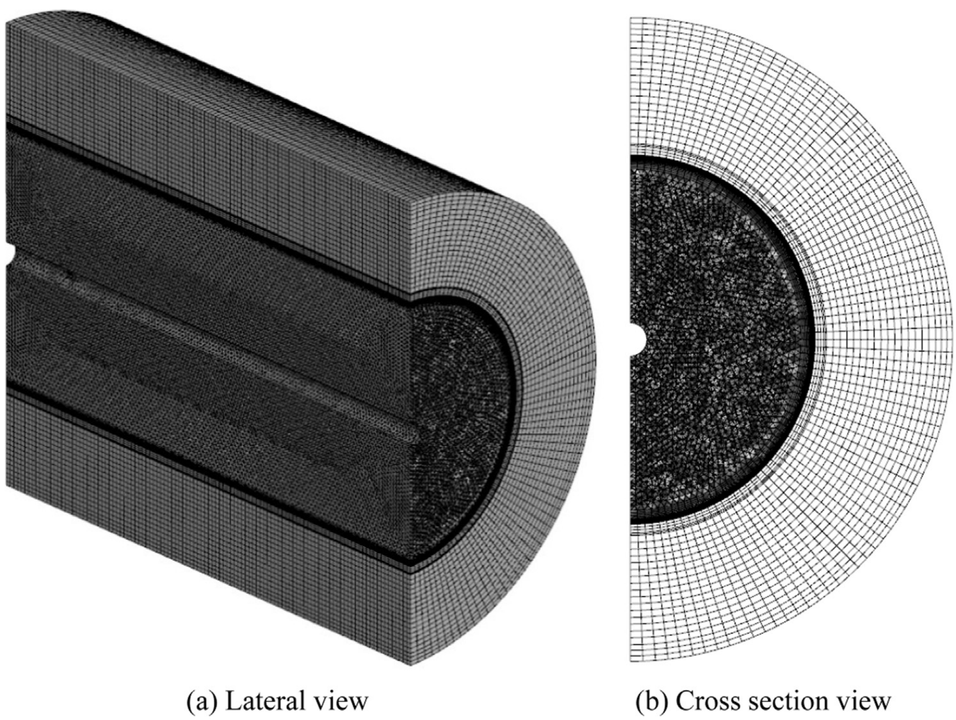

Fig. 3. Grid system.

Table 3
Mesh independence test.

Working conditions: $\dot{m} = 0.57$ kg/s, $d = 20$ mm, $\beta = 50^\circ$, $p^* = 2$, $T_{inlet} = 400$ K					
Model	Grid number	Nu	f	Average temperature of absorber tube inner wall T_w (K)	Maximum temperature of absorber tube inner wall T_{max} (K)
1	438391	170.90	0.308604	526.92	631.93
2	972539	171.75	0.310876	525.95	630.33
3	1518546	171.96	0.309138	525.75	630.04

3.1. Governing equations

In this study, all Reynolds numbers used are greater than 5000, and thus, the flow is in the fully developed turbulent regime. A realizable k-ε turbulent model [35] is applied in the present study owing to its superior performance in predicting the flow features including strong streamline curvature, vortices and rotation [36]. For a more detailed description of the model, please refer to the Ref. [31].

3.2. Boundary conditions and solution procedure

The cross-section of a solar PTR and the corresponding thermal network are displayed in Fig. 2. The heat transfer in this study is complex and the whole research object includes three types of heat transfer modes: conduction, convection and radiation. The direct and concentrated solar radiation that irradiates the absorber tube outer surface is absorbed by a selective coating and converted into heat. The

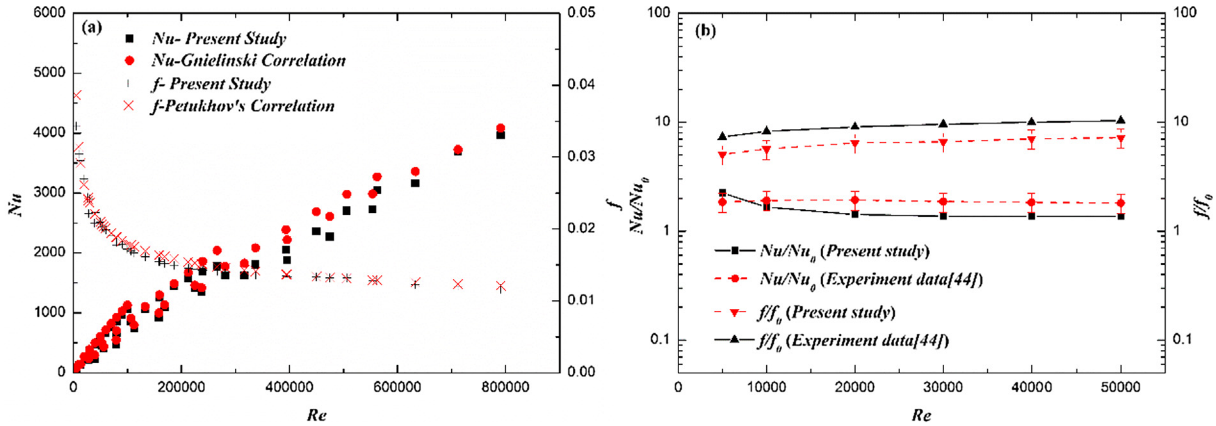

Fig. 4. Validation of heat transfer and fluid friction factor performance, (a) smooth PTR, (b) PTR with inserts.

Table 4
Validation of heat gain and collector efficiency.

case	1	2	3	4	5	6	7	8
DNI (W/m^2)	933.7	968.2	982.3	909.5	937.9	880.6	920.9	903.2
Wind speed (m/s)	2.6	3.7	2.5	3.3	1.0	2.9	2.6	4.2
Air temperature (°C)	21.2	22.4	24.3	26.2	28.8	27.5	29.5	31.1
Flow rate (L/min)	47.70	47.78	49.10	54.70	55.50	55.60	56.80	56.30
T_{inlet} (°C)	102.2	151.0	197.5	250.7	297.8	299.0	379.5	355.9
ΔT (°C) (Experiment)	21.80	22.02	21.26	18.70	19.10	18.20	18.10	18.50
ΔT (°C) (Present study)	21.71	22.43	22.25	18.68	19.20	17.94	18.71	18.42
Error ΔT(%)	−0.41	1.85	4.66	−0.11	0.51	−1.41	3.40	−0.41
Efficiency (Experiment)	72.51	70.90	70.17	70.25	67.98	68.92	62.34	63.83
Efficiency (Present study)	71.67	71.13	70.52	69.41	67.87	67.61	63.21	64.77
Error efficiency (%)	−1.15	0.32	0.50	−1.19	−0.17	−1.90	1.40	1.47

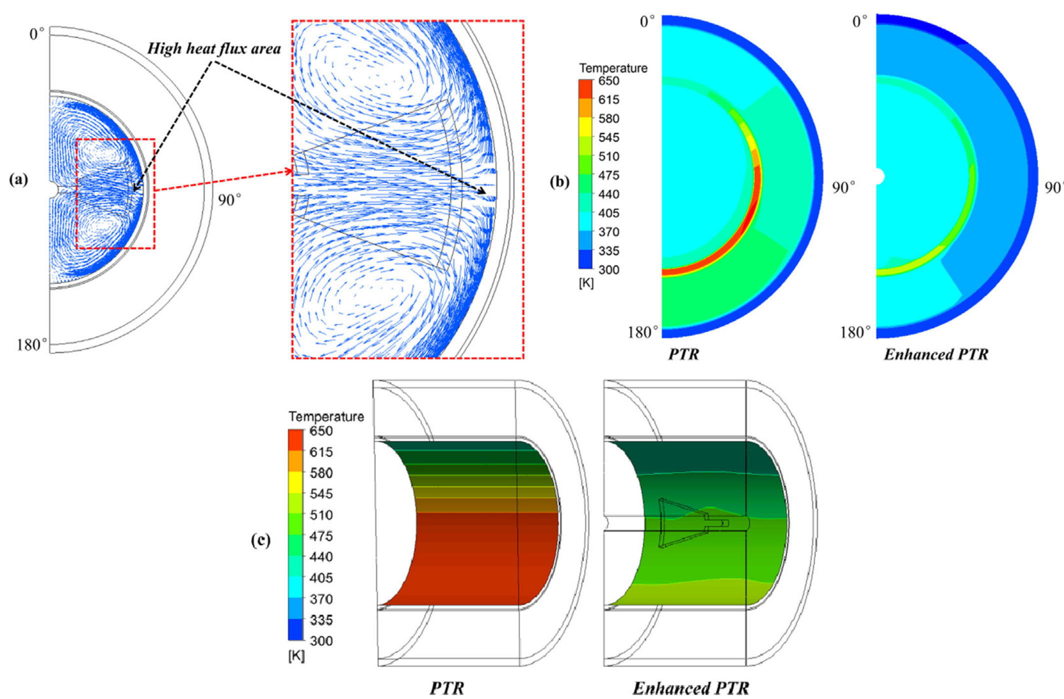

Fig. 5. Flow field of the enhanced PTR and comparison of temperature distribution between the smooth PTR and enhanced PTR at T_{inlet} = 400 K, Re = 10,000, p^* = 1, d = 20 mm, and β = 40°: (a) tangential velocity vectors on the cross-section of the enhanced PTR; (b) temperature distributions on the cross-section; (c) temperature distributions on the absorber tube's inner wall.

concentrated solar radiation is almost loaded in the lower half of the absorber tube. Thus, the absorber tube outer surface receives a non-uniform heat flux. The heat flux distribution with a rim angle equal to 80° from the work of Mwesigye et al. [37] is applied as the thermal boundary condition in the absorber tube outer wall, and its Fourier formulas are listed in Table 1. The direct normal irradiance (DNI) is 1000 W/m^2.

Most of the heat loaded on the outer wall of the absorber tube is

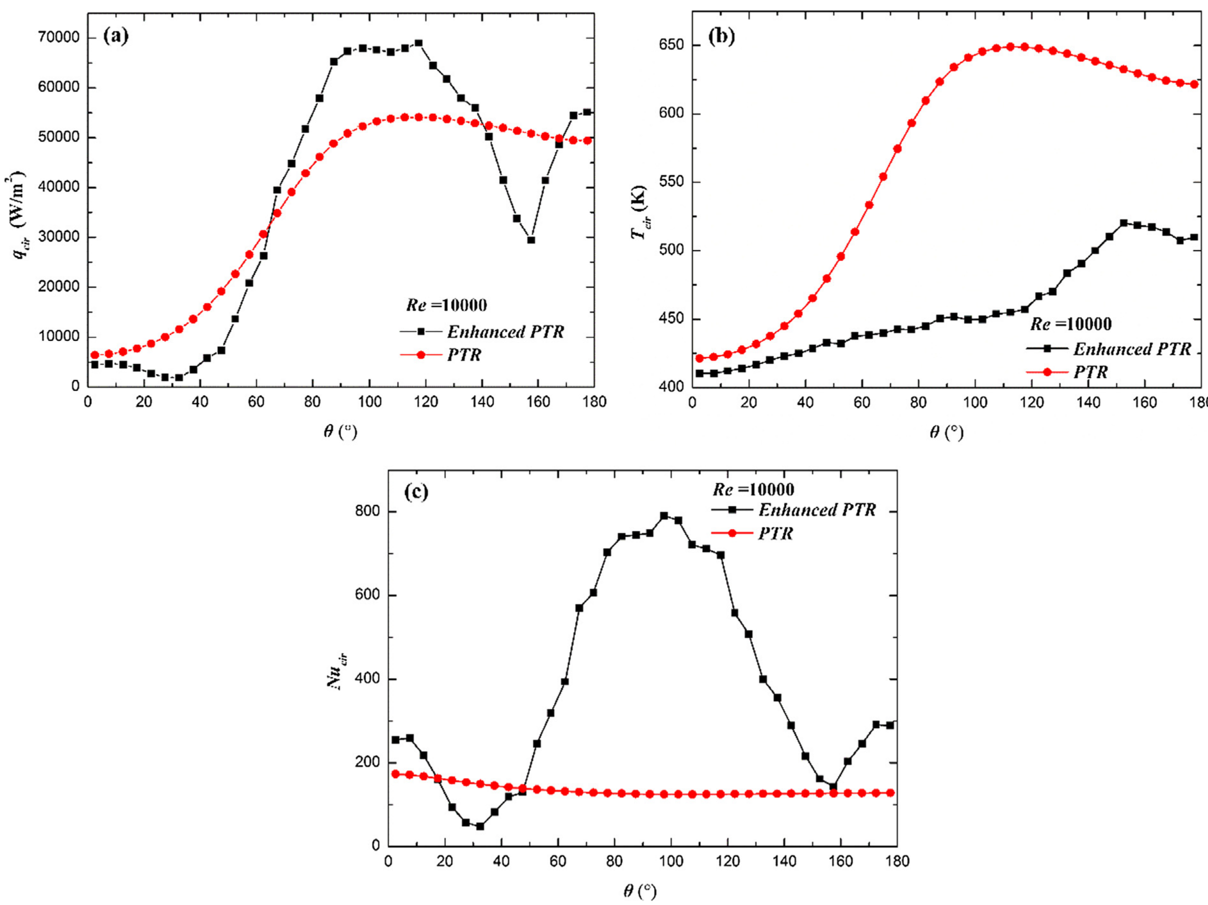

Fig. 6. Quantitative comparisons of circumferential variables on the absorber tube's inner wall between PTR and enhanced PTR ($p^* = 1$, $d = 20$ mm and $\beta = 40°$) under $T_{inlet} = 400$ K and $Re = 10{,}000$: (a) circumferential heat flux; (b) circumferential temperature; (c) circumferential Nusselt number.

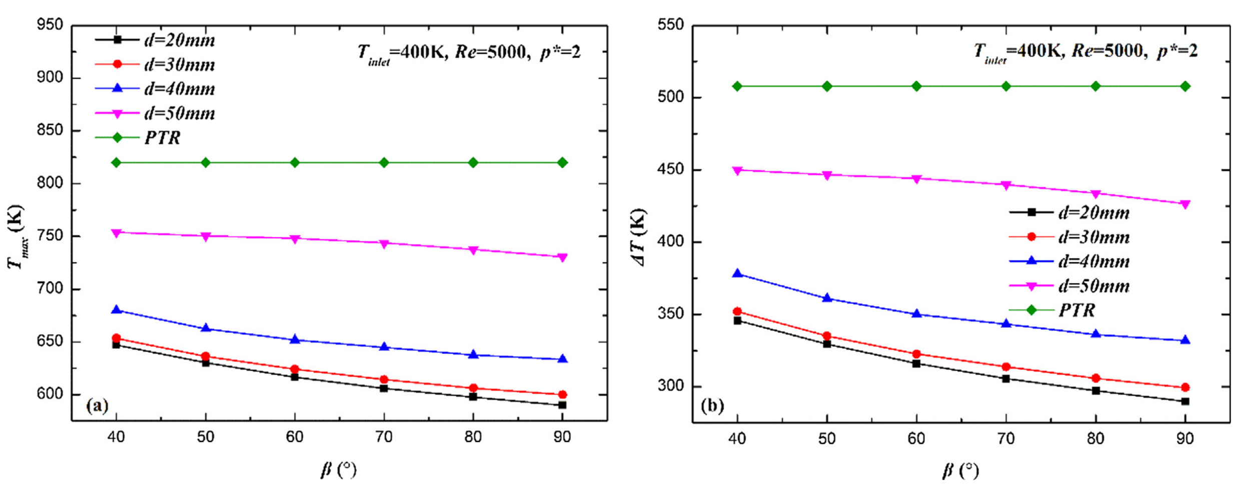

Fig. 7. Variations in absorber tube temperatures with central angle at different hollow diameters: (a) peak temperature; (b) temperature gradient.

conducted to the inner wall, and then carried away by HTF through heat convection. Stainless steel (321H) is adopted as the absorber tube material with a thermal conductivity of 25 $\mathrm{W m^{-1} K^{-1}}$. Table 2 lists the temperature-dependent properties of Syltherm-800, which is applied as the HTF in the present study. The inlet and outlet of the absorber tube are set as translational periodic boundary conditions. The inner wall of absorber tube and surface of the inserts are set as a no-slip boundary condition. To investigate the effect of fluid temperature on PTR performance, four fluid inlet temperatures of 400, 500, 600, and 650 K are applied. In addition, the mass flow rate ranges from 0.57 to 11.40 kg/s, with the Reynolds number ranging from 5000 to 791,000 under different fluid temperatures, and the corresponding fluid velocities range from 0.2 to 5.7 m/s.

The remaining heat is transferred to the inner surface of the glass cover by heat radiation and conduction when there is little gas in the annular space. The radiation heat transfer through the annular space is simulated using a discrete ordinates (DO) radiation model. The temperature-dependent emissivity of the coating on the tube's outer wall is formulated as Eq. (1) [31], where T is the absorber tube temperature in K. The glass cover is assumed as a gray body and the emissivity of the

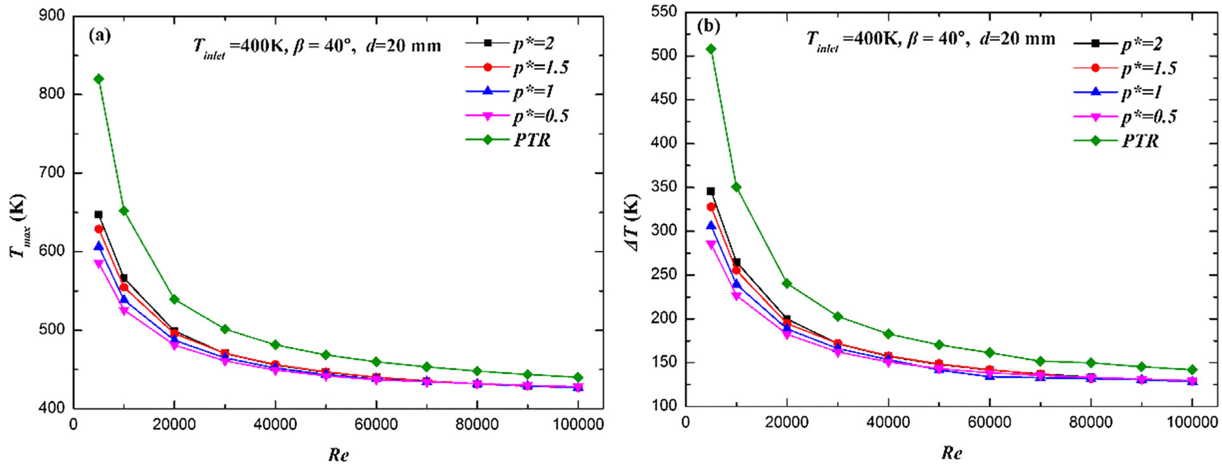

Fig. 8. Variations in absorber tube temperatures with Reynolds number at different pitch ratios: (a) peak temperature; (b) temperature gradient.

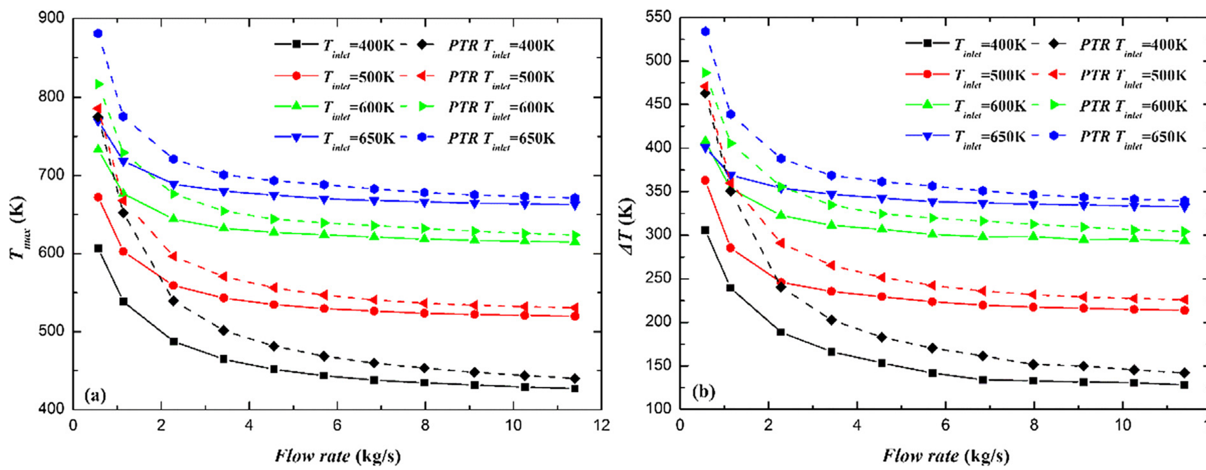

Fig. 9. Variations in absorber tube temperatures with mass flow rate for different fluid inlet temperatures: (a) peak temperature; (b) temperature gradient.

glass inner surface is set to 1.

$$\xi = 0.000327T - 0.065971 \tag{1}$$

The heat, that is transferred from the absorber tube outer surface to the glass inner surface, is conducted to the glass outer surface and then released to the environment through convection and radiation. Pyrex is adopted as the glass cover material, with a thermal conductivity of $1.2\,\mathrm{W\,m^{-1}\,K^{-1}}$. A mixed boundary condition is used on the outer surface of the glass cover. The net heat flux through radiation is calculated according to the Stefan-Boltzmann law. The glass outer surface external emissivity is 0.89. In this study, the ambient temperature is set to 298 K and the sky temperature is set to 290 K, which is 8 K lower than the ambient temperature [38]. According to the study of Song et al. [29], the emissivity of the sky is 0.79. An assumption of a uniform convection boundary condition is adopted in this study and the convective heat transfer coefficient is defined as follows [39]:

$$h_w = 4{V_w}^{0.58}{d_{go}}^{-0.42} \tag{2}$$

where V_w is the wind speed which is assumed to be 2.5 m/s in this study.

The governing equations are implemented using the ANSYS Fluent 15.0 software, which is based on the finite volume method. A second-order upwind scheme is employed to discretize the governing equations for momentum and energy while the SIMPLE algorithm is applied to achieve the coupling between velocity and pressure. The enhanced wall treatment method is used to capture the high resolution of gradients in the region near the tube wall. The convergence criterion in this study states that the relative residual values are less than 10^{-4} for the continuity equation and less than 10^{-7} for all other variables, or all the relative residual values are maintained constant.

3.3. Parameter definitions

The Reynolds number (*Re*) is defined as:

$$\mathrm{Re} = \frac{u_{inlet}d_{ri}}{\nu} \tag{3}$$

where u_{inlet} is the average velocity at the inlet, and ν is the kinematic coefficient of the viscosity of HTF.

The definitions of heat transfer coefficient (h) and average Nusselt number (Nu) are expressed formulas as follows:

$$h = q/(T_W - T_f) \tag{4}$$

$$Nu = hd_{ri}/\lambda \tag{5}$$

where q and T_w are the average heat flux and average temperature on the inner wall of the absorber tube, respectively. Term T_f is the mean temperature of the fluid which is calculated from the arithmetic mean of the inlet and outlet mass-average temperatures. Term λ is the thermal conductivity of HTF.

The friction factor (f) is given by:

$$f = \frac{2\Delta P d_{ri}}{\rho u_{inlet}^2 L} \tag{6}$$

where ΔP is the pressure drop between the inlet and outlet of the

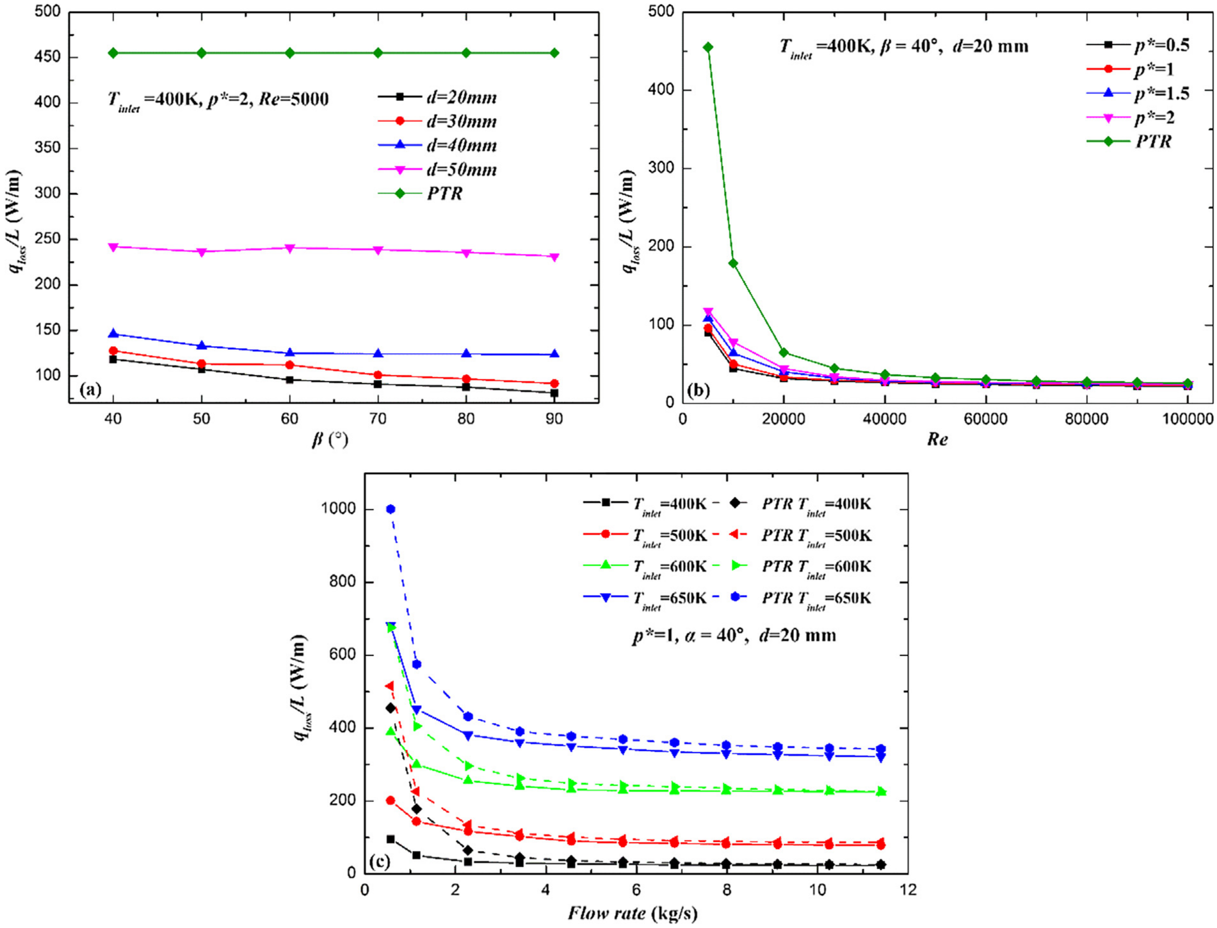

Fig. 10. Effects of parameters on the heat loss of receiver: (a) effects of central angle and hollow diameter; (b) effect of pitch ratio; (c) effect of fluid inlet temperature.

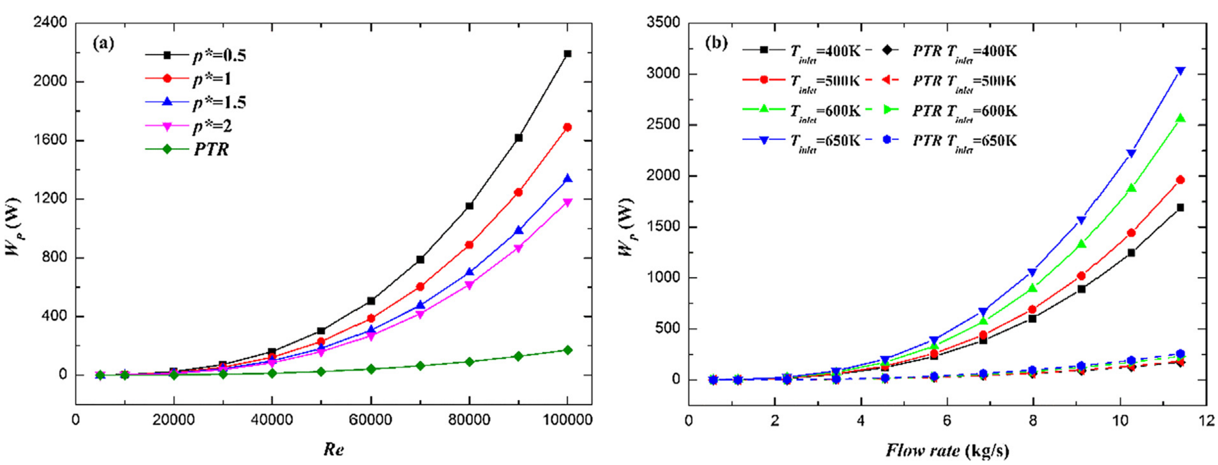

Fig. 11. Variations in pumping work with (a) Reynolds number for different pitch ratios and (b) mass flow rate at different fluid inlet temperatures.

absorber tube, and ρ is the density of the HTF.

A performance evaluation criteria (*PEC*) is applied to evaluate the overall thermal-hydraulic performance of the heat convection process of PTR under the given pumping power, which is defined as [40]

$$PEC = \frac{Nu/Nu_0}{(f/f_0)^{1/3}} \tag{7}$$

where Nu and f represent the average Nusselt number and friction factor of the enhanced PTR, and Nu_O and f_O are the average Nusselt number and friction factor of the smooth PTR, respectively.

To analyze the temperature distribution and heat transfer performance along the circumference, the circumferentially average temperature T_{cir} and Nusselt number Nu_{cir} of the inner wall of the absorber tube are defined as follows[27]:

$$T_{cir} = \frac{1}{L\Delta\theta}\int_0^L \int_{\theta_i}^{\theta_i+\Delta\theta} T_w d\theta dz \tag{8}$$

$$Nu_{cir} = \frac{1}{L\Delta\theta}\int_0^L \int_{\theta_i}^{\theta_i+\Delta\theta} Nu d\theta dz \tag{9}$$

Entropy generation analysis is applied in this study to evaluate the thermodynamic performance of PTR. The entropy generation rate from the fluid friction irreversibility S'^{F}_{gen} and the heat transfer irreversibility

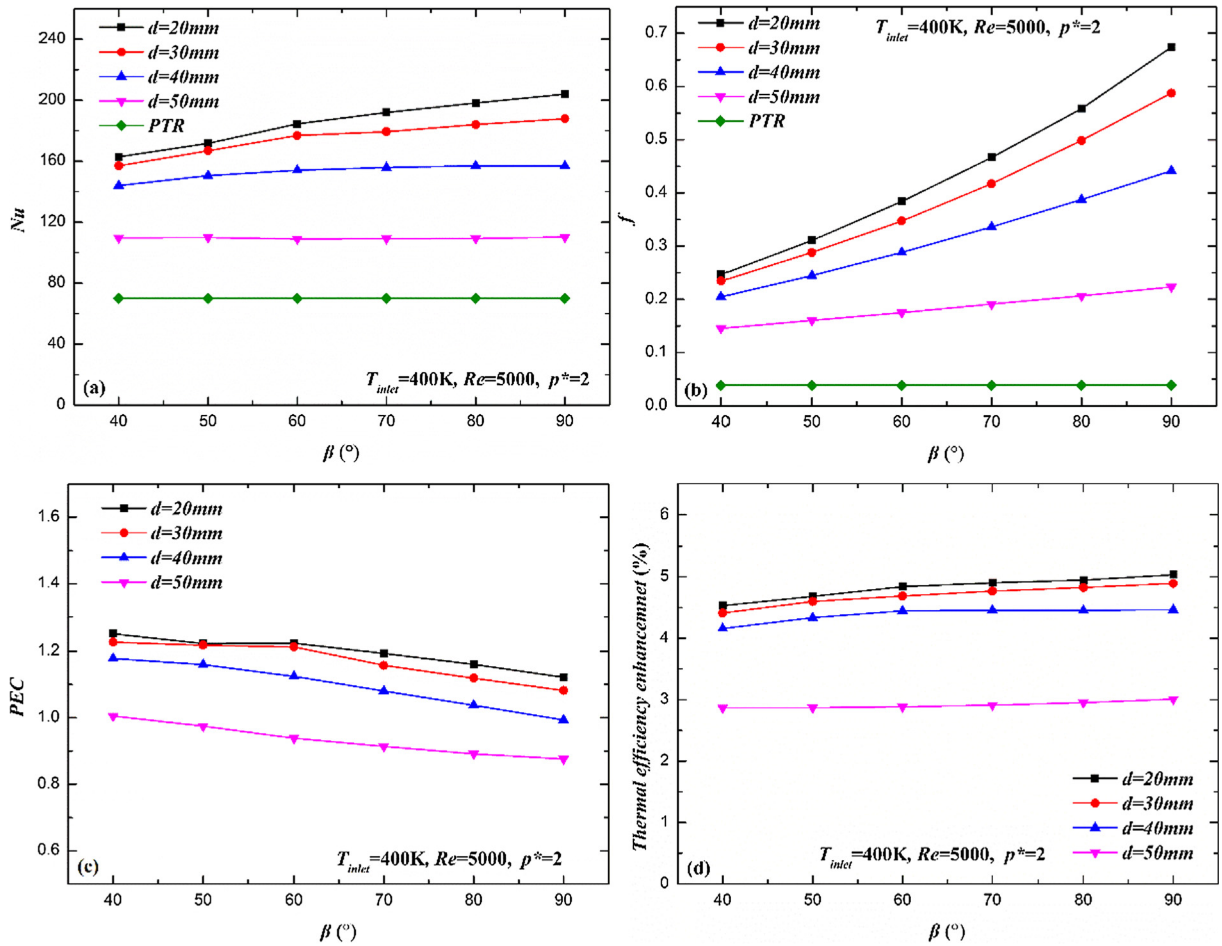

Fig. 12. Variations in thermal-hydraulic performance at different hollow diameters with central angle: (a) Nusselt number; (b) friction factor; (c) *PEC* value; (d) thermal efficiency enhancement.

S'^{H}_{gen} per unit volume are given by Eqs. (10) and (11).

$$S'^{F}_{gen} = \frac{\mu}{T}\left(\frac{\partial u_i}{\partial x_j} + \frac{\partial u_j}{\partial x_i}\right)\frac{\partial u_i}{\partial x_j} + \frac{\rho\varepsilon}{T} \tag{10}$$

$$S'^{H}_{gen} = (1 + \frac{\alpha_t}{\alpha})\frac{\lambda}{T^2}(\nabla T)^2 \tag{11}$$

The total entropy generation rate can be achieved from the volume integral of the entropy generation rate per unit, formulas follows:

$$S_{gen} = S_{gen}{}^{F} + S_{gen}{}^{H} = \frac{1}{V}\int\int\int_V S'^{F}_{gen}dV + \frac{1}{V}\int\int\int_V S'^{H}_{gen}dV \tag{12}$$

The entropy generation ratio ($N_{S,en}$) is defined as follows:

$$N_{S,\mathrm{en}} = S_{gen}/(S_{gen})_0 \tag{13}$$

where $(S_{gen})_0$ is the total entropy generation rate of the corresponding smooth PTR.

3.4. Mesh generation and independence test

In this study, the commercial software Gambit 2.4.6 is applied to generate a three-dimensional grid model, which is shown in Fig. 3. Tetrahedral elements with highly refined grids in the region near the absorber tube inner wall are adopted for CFD simulation of the HTF domain, while structured hexahedral meshes are generated for CFD analysis of the absorber tube, vacuum, and glass cover domains.

A grid independence test is carried out at $\dot{m} = 0.57$ kg/s, $d = 20$ mm, $\beta = 50°$, $p^* = 2$, and $T_{inlet} = 400$ K. To test the accuracy of the numerical simulations, three grid models are applied for independence test, whose results are presented in Table 3. The grid model 2 is sufficiently dense and is employed in the present study, because the deviations of *Nu*, *f*, average temperature, and maximum temperature of absorber tube inner wall are less than 1%.

4. Model validation

Petukhov's correlation for the friction factor and the Gnielinski correlation for the Nusselt number, which are given in Eqs. (14) and (15), are applied to validate the heat transfer and flow resistance performance of a smooth PTR. Good agreements are obtained, with the deviations between simulations and correlations within 14.1% for the Nusselt number and 11.1% for the friction factor, as shown in Fig. 4(a). In Fig. 4(b), the simulated results are compared with the experimental data of similar inserts [41]. The relative deviations are 26.5% for Nusselt number ratios and 31.1% for friction factor ratios. Considering the unavoidable discrepancies between the numerical methods and experimental measurements, such as differences in working fluid and geometry of inserts, as well as the uncertainty of the experimental measurements (approximately ± 20%), the numerical model adopted in this study has a reasonable accuracy. Furthermore, the temperature gain and collector efficiency of a receiver without inserts are compared with experimental data from Dudley et al. [42] to verify the calculation accuracy of the model, as listed in Table 4. Good agreement is obtained as the deviations are less than ± 4.7% for temperature gain and less than ± 1.5% for collector efficiency. Note that all conditions of the numerical model and experiments in Dudley's work are the same except

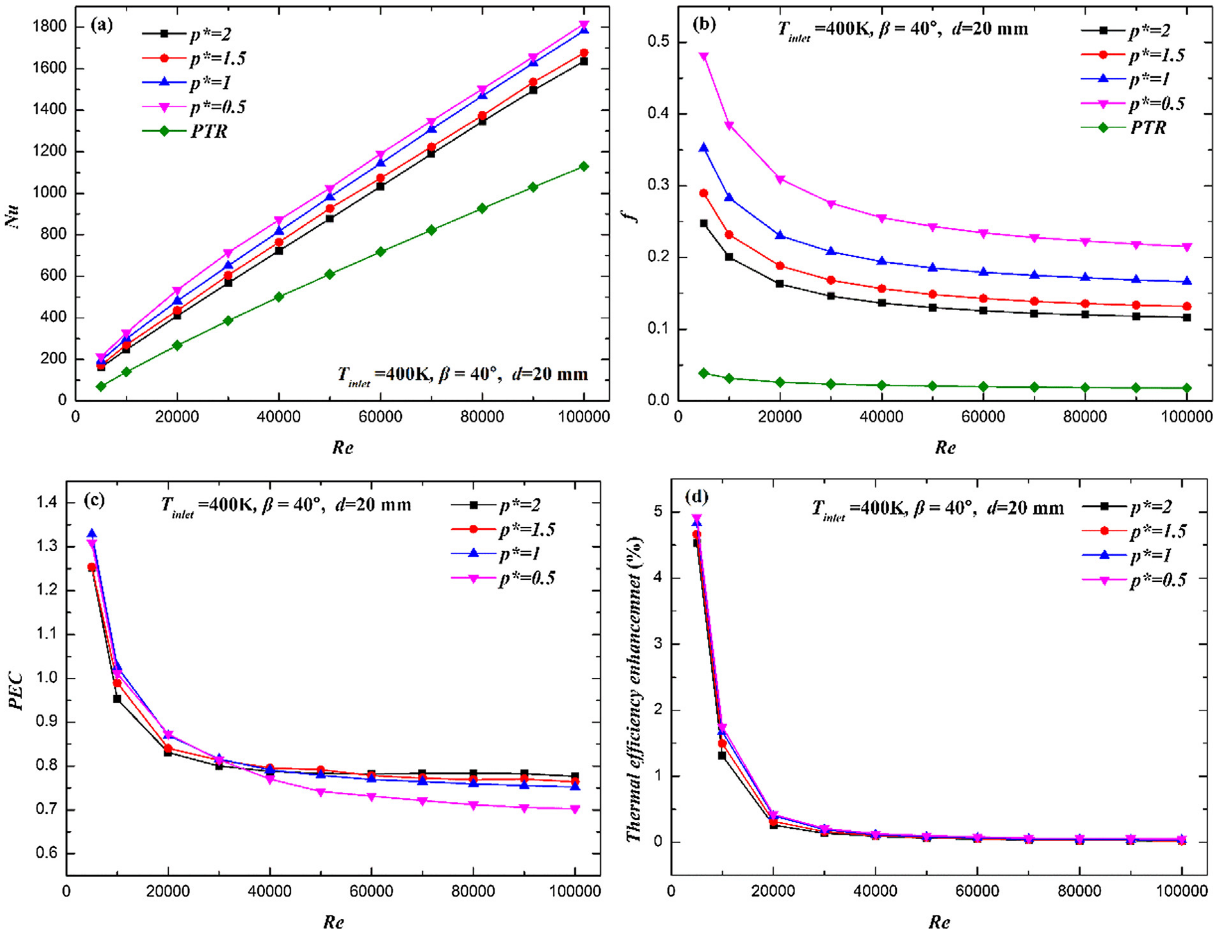

Fig. 13. Effects of pitch ratio on thermal-hydraulic performances: (a) Nusselt number; (b) friction factor; (c) *PEC* value, (d) thermal efficiency enhancement.

that the rim angle is 80° in the numerical model and 70° in the experiments. According to He et al. [43], the effect of rim angle on temperature gain is extremely limited when rim angle ranges from 30° to 90°. Therefore, to some extent, the numerical model can be validated by the experimental data.

$$f = (0.790\ln \mathrm{Re} - 1.64)^{-2} \tag{14}$$

$$Nu = \frac{(f/8)(\mathrm{Re}-1000)\mathrm{Pr}}{1 + 12.7(f/8)^{0.5}(\mathrm{Pr}^{2/3} - 1)} \tag{15}$$

5. Results and discussion

A comprehensive discussion on flow field, heat transfer performance and temperature distribution, which are the most important factors affecting the overall efficiency and thermal and mechanical performance of PTR, are performed in this section. Effects of parameters and entropy and exergy analysis are also discussed. In addition, comparisons with other published works and limitations of this study are added to the last part of this section.

5.1. Flow field and temperature distribution

Fig. 5(a) shows the tangential velocity vectors on the cross-section of the absorber tube with conical strip inserts. Clearly, the conical strip inserts generate a pair of vortexes in the absorber tube flow, which allows a rapid and sufficient exchange and mixing of the cold fluid in the core region and the hot fluid at the boundary, and consequently enhances the convection heat transfer between the HTF and absorber tube inner wall. Especially, the conical strip inserts guide the cold fluid to flush the absorber tube inner wall for θ ranging from 70° to 110°, which exactly covers the high heat flux area (approximately θ = 88.6°). As a result, the heat in the high heat flux area can be rapidly taken away and the peak temperature that exists on the tube wall of the smooth PTR can be significantly reduced. Fig. 5(b) and (c) display comparisons of temperature distributions on the cross-section and the absorber tube inner wall between the smooth PTR and enhanced PTR. As expected, the temperatures in the absorber tube of the enhanced PTR are effectively reduced. In addition, the temperature in the glass cover of the enhanced PTR also decreases, resulting in a significant reduction in heat loss.

Fig. 6 displays comparisons of the circumferentially average heat flux (q_{cir}), temperature (T_{cir}), and Nusselt number (Nu_{cir}) on the absorber tube inner wall. The heat flux on the tube inner wall in the area with θ ranging from 70° to 140° of the enhanced PTR is increased compared to the smooth PTR, due to a strong fluid impingement on this area. Meanwhile, because of the strong fluid impingement, the temperature in this area of the enhanced PTR is apparently lower than that of the smooth PTR, as shown in Fig. 6(b). Moreover, the circumferential temperature gradient of absorber tube for the enhanced PTR is significantly decreased, compared to that of smooth PTR, which is beneficial for reducing the thermal stress and deformation of the absorber tube. According to Fig. 6(c), although the local Nusselt number in the area with θ ranging from 18° to 50° of the enhanced PTR is lower than that of the smooth PTR, the local Nusselt number in the area with θ ranging from 70° to 140° of the enhanced PTR is much higher than that of the smooth PTR. As a result, the global-average Nusselt number of the enhanced PTR is approximately 2.2 times that of the smooth PTR, which means that the conical strip inserts can effectively improve the PTR performance.

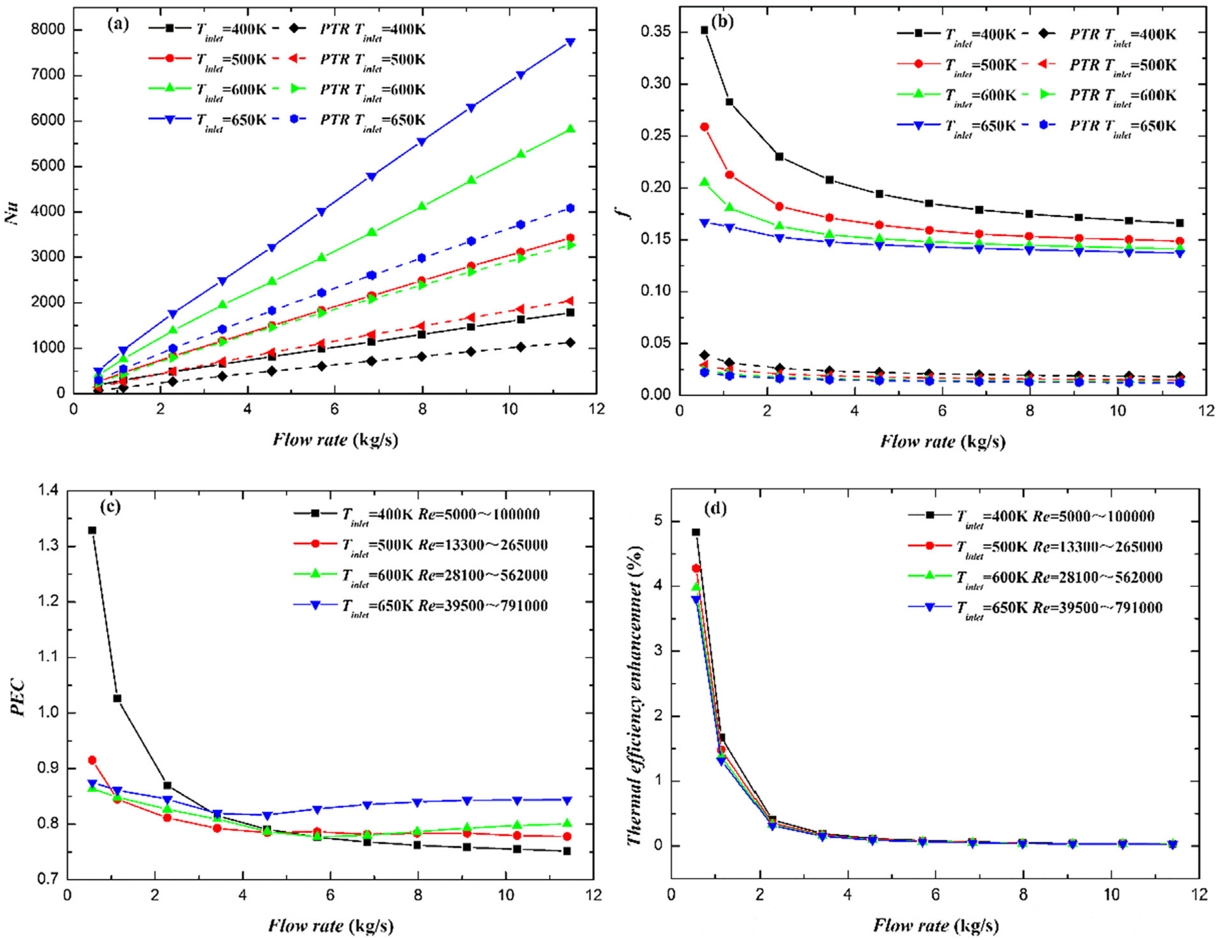

Fig. 14. Variations of thermal-hydraulic performances with mass flow rate at d = 20 mm, β = 40° and p^* = 2 for different fluid inlet temperatures: (a) Nusselt number; (b) friction factor; (c) *PEC* value; (d) thermal efficiency enhancement.

5.2. Temperatures of absorber tube and heat loss

Generally, one of the purposes of enhancing heat transfer for a PTR is to reduce the temperatures (especially the peak temperature) and temperature gradient in the absorber tube to achieve the following benefits: (1) avoiding or minimizing degradation of the HTF; (2) reducing heat loss of the receiver; and (3) reducing thermal stresses in the absorber tube and improving operational safety of the PTR. Figs. 7–9 show the effects of the parameters on the absorber tube peak temperature and temperature gradient. Term ΔT is the difference between the maximum and minimum temperatures of the absorber tube inner wall. It is clear that both peak temperature and temperature gradient are significantly reduced by the conical strip inserts, compared to the smooth PTR. Both the peak temperature and temperature gradient decrease with a decrease of hollow diameter and increase in the central angle, as shown in Fig. 7. Moreover, both the peak temperature and temperature gradient of the absorber tube decrease with the pitch ratio and increase with the fluid inlet temperature, as shown in Figs. 8 and 9. Furthermore, as the Reynolds number or mass flow rate increases, the reductions in peak temperature and temperature gradient decrease. In addition, the deviations between different pitch ratios decrease gradually with the Reynolds number.

To analyze the heat loss of PTR, Fig. 10 shows the effects of the parameters on heat loss of the receiver. As expected, the variations in heat loss are the same as those in the absorber tube temperatures. The heat loss tends to decrease with the central angle but increase with the hollow diameter, pitch ratio, and fluid inlet temperature. In addition, compared to the smooth PTR, the heat loss is significantly reduced by the conical strip inserts, especially at low Reynolds numbers or mass flow rates.

5.3. Pumping work demand

Fig. 11 displays the variation of pumping work demand with Reynolds number and mass flow rate under different parameters. It is found that the pumping work demand increases with the decrease of pitch ratio under the same Reynolds number and the increase of the inlet temperature under the same mass flow rate. Especially, the pumping work demand increases more and more rapidly with the Reynolds number and/or mass flow rate. The pumping work demand of the system is ranged in 0.03–257.30 W for the smooth absorber tube and 0.24 to 3042.37 W for the absorber tube with inserts. Therefore, the huge pumping work demand at high Reynolds number or mass flow rate is difficult to meet in practical applications, and the enhanced PTRs are only suitable for application at low Reynolds number or flow rate.

5.4. Effects of parameters on thermal-hydraulic performances

Fig. 12 displays the variations in Nusselt number, friction factor, and *PEC* with increasing central angle (β) under the conditions of T_{inlet} = 400 K, Re = 5000 and p^* = 2. In general, the stronger the disturbance in the fluid, the higher is the heat transfer efficiency obtained. Fig. 12(a) clearly shows that the Nusselt number decreases with the hollow diameter (d) and increases slightly with the central angle (β). In addition, the larger the hollow diameter, the smoother the Nusselt number increases with the central angle. At the same time, the

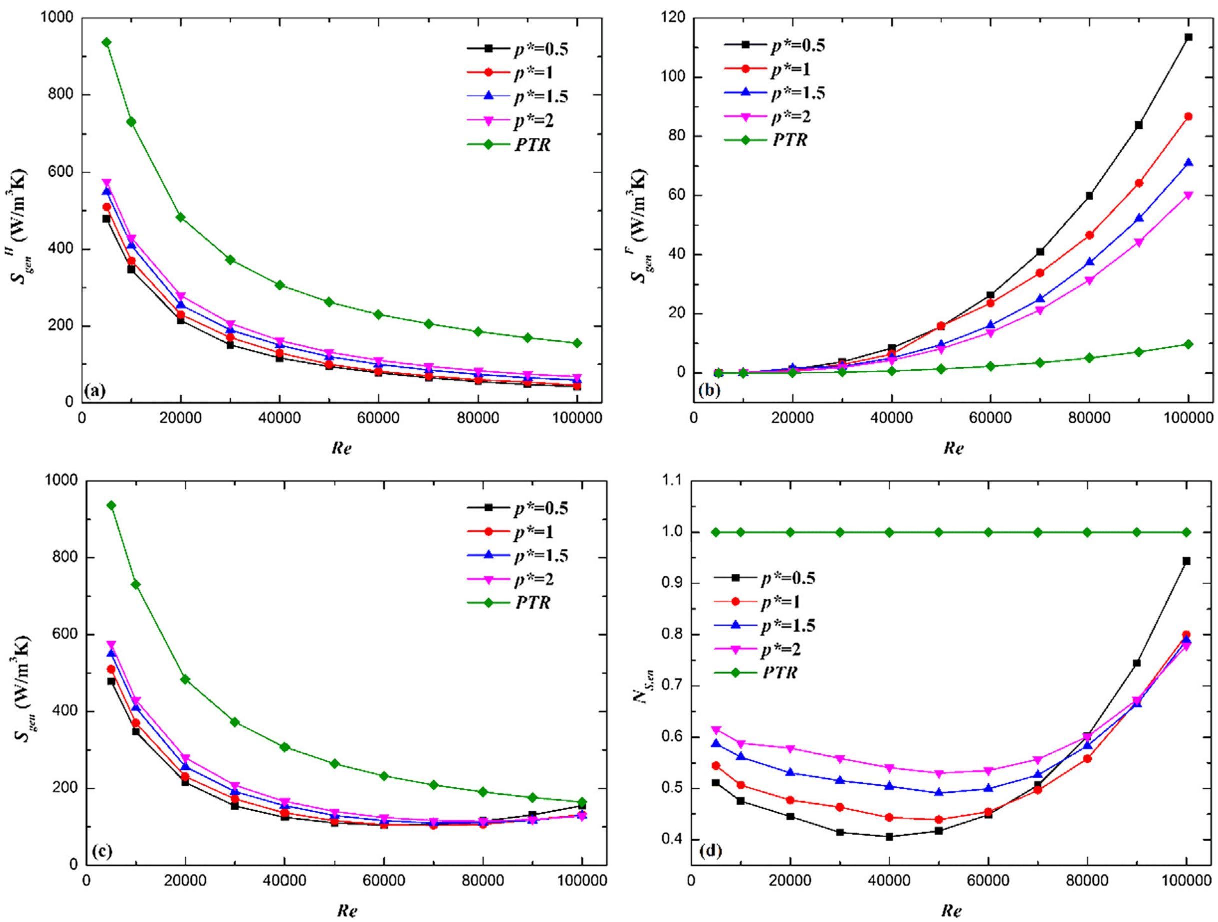

Fig. 15. Variations in entropy generations and entropy generation ratio with Reynolds number for different pitch ratios: (a) entropy generation from the heat transfer irreversibility; (b) entropy generation from the fluid friction irreversibility; (c) total entropy generation; (d) entropy generation ratio.

disturbance in the fluid causes a significant increase in the flow resistance compared to the smooth PTR. As shown in Fig. 12(b), the friction factor increases considerably with a decrease in the hollow diameter and an increase in the central angle. When considering the overall thermal-hydraulic performance, *PEC* decreases with an increase in both the hollow diameter and central angle, as shown Fig. 12(c). Especially, the *PEC* values are less than 1 when d = 50 mm, which means that the increase in pumping power outweighs the enhancement in heat transfer and there is no overall enhancement in heat transfer. Therefore, the application of inserts with larger hollow diameter should be avoided. Fig. 12(d) shows that the thermal efficiency enhancement decreases with the increasing hollow diameter and increases slightly with the central angle.

The effects of pitch ratio on heat transfer, flow resistance, and overall thermal-hydraulic performance at T_{inlet} = 400 K, β = 40°, and p^* = 2 are presented in Fig. 13(a)–(d), respectively. Both the Nusselt number and friction factor increase as the pitch ratio decreases, and the friction factor is more sensitive to the pitch ratio than the Nusselt number. Fig. 13(c) demonstrates that the *PEC* value decreases with the Reynolds number. Moreover, the smaller the pitch ratio, the faster the PEC value decreases with the Reynolds number. Therefore, conical strip inserts with a small pitch ratio can obtain a higher *PEC* value at a low Reynolds number, while the inserts with a large pitch ratio can obtain a higher *PEC* value at a high Reynolds number. The result that the *PEC* value is less than 1 at a high Reynolds number indicates that the insert is more suitable for lower Reynolds number situations. Great thermal efficiency enhancements at low Reynolds numbers are obtained due to the significant reduction in heat loss at low Reynolds number or mass flow rate. The thermal efficiency enhancement decreases sharply with an increase in the Reynolds number and increases with decreasing pitch ratio, as shown in Fig. 13(d).

Because the properties of the HTF have strong temperature dependence, the fluid inlet temperature has a significant impact on its flow and heat transfer performance. Therefore, it is necessary to study the thermal-hydraulic performance at different fluid inlet temperatures. Fig. 14(a)–(d) show the variations in Nusselt number, friction factor, *PEC* value and thermal efficiency enhancement with the mass flow rate at d = 20 mm, β = 40° and p^* = 2 for different fluid inlet temperatures, respectively. The Reynolds number increases with the fluid inlet temperature at the same mass flow rate. As a result, the Nusselt numbers of both the enhanced PTR and smooth PTR increase with the fluid inlet temperature, as shown in Fig. 14(a). Furthermore, compared to the smooth PTR, the heat transfer performance of the enhanced PTR is effectively improved by the conical strip inserts, with the Nusselt number ranging from 1.56 to 2.77 times that of the smooth PTR. At the same time, the friction factors of both the enhanced PTR and smooth PTR decrease with the fluid inlet temperature, and the flow resistance is significantly increased by the conical strip inserts with the friction factor ranging from 7.55 to 11.35 times that of the smooth PTR, as shown in Fig. 14(b). Fig. 14(c) shows that the *PEC* value decreases with the mass flow rate at low fluid inlet temperatures (T_{inlet} = 400 and 500 K), while it decreases first and then increases slightly with the mass flow rate at high fluid inlet temperatures (T_{inlet} = 600 and 650 K). Moreover, when the mass flow rate is low (lower than approximately 3.5 kg/s), the case with low fluid inlet temperature can obtain a higher *PEC* value, while when the mass flow rate is high, the case with a high fluid inlet temperature can obtain a higher *PEC* value. The *PEC* values ranges from 0.75 to 1.33. Fig. 14(d) demonstrates that the thermal

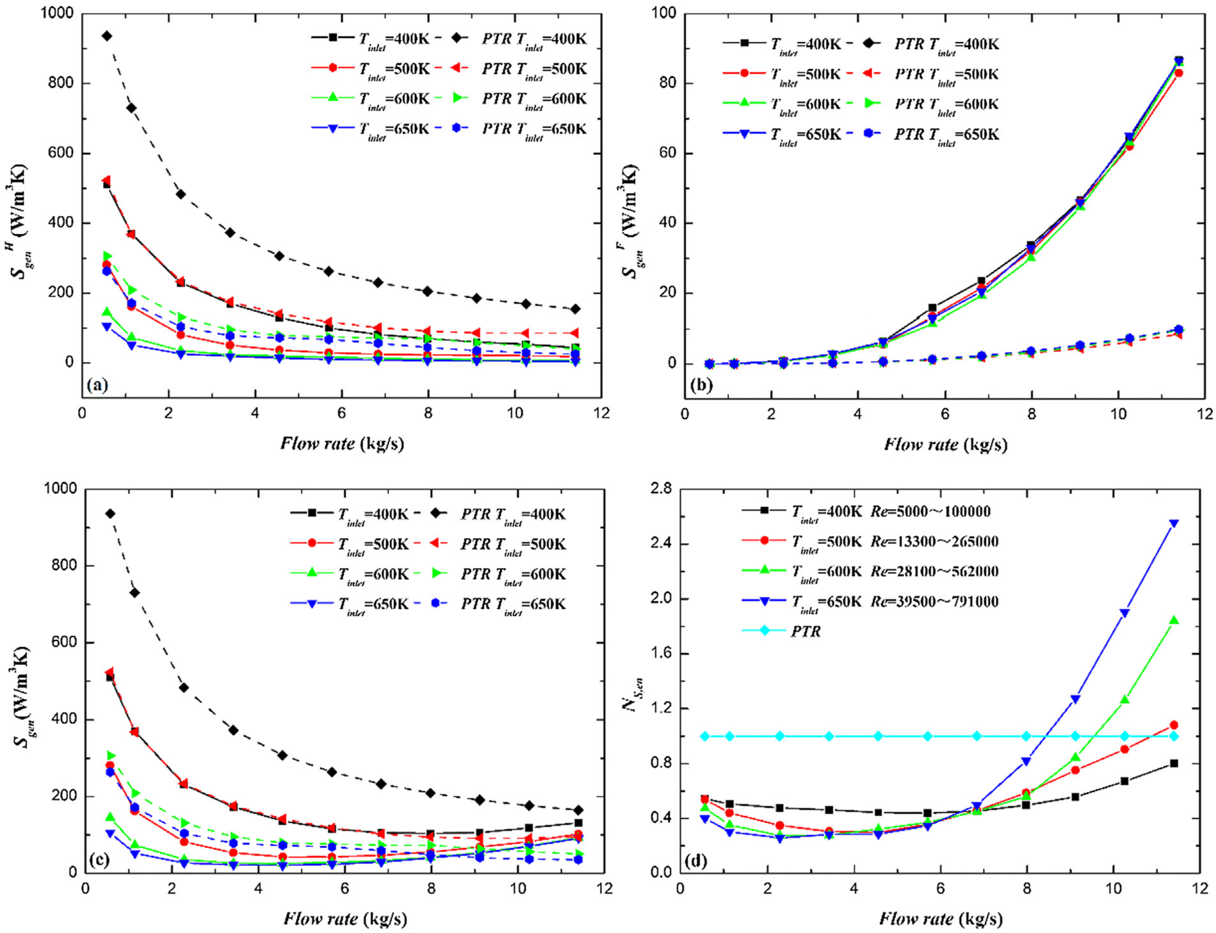

Fig. 16. Variations in entropy generations and entropy generation ratio with mass flow rate at different fluid inlet temperatures: (a) entropy generation from heat transfer irreversibility; (b) entropy generation from fluid friction irreversibility; (c) total entropy generation; (d) entropy generation ratio.

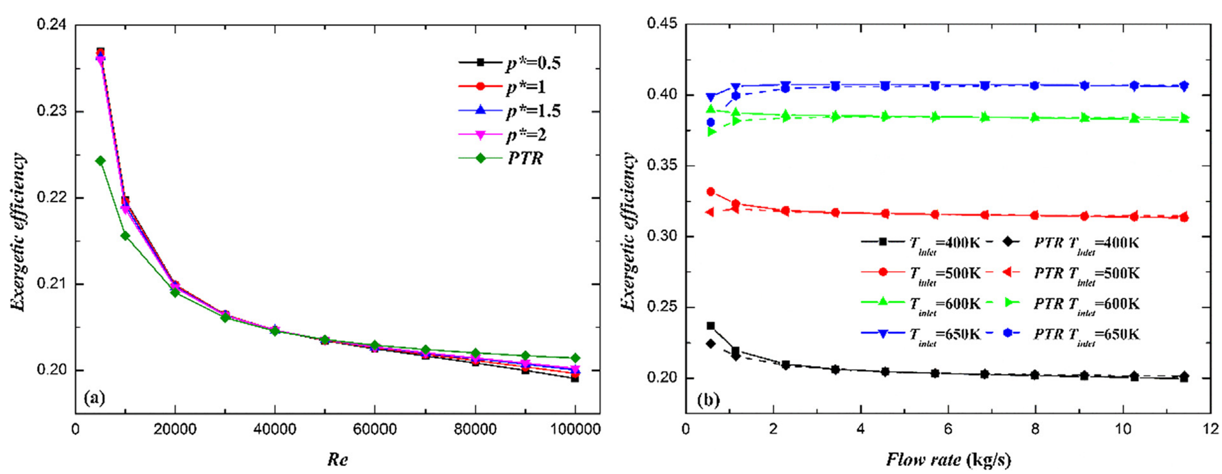

Fig. 17. Variations in exergetic efficiencies with (a) Reynolds number for different pitch ratios and (b) mass flow rate at different fluid inlet temperatures.

efficiency enhancement decreases with the increase of mass flow rate and the increase of the fluid inlet temperature at the same flow rate. And it is ranged in 0.03–4.83%.

5.5. Entropy and exergy analysis

To evaluate the thermodynamic performance of the conical strip inserts, entropy analysis is conducted in this study. The conical strip inserts can enhance the thermodynamic performance when the entropy generation ratio $N_{S,en}$ is less than 1. Fig. 15 displays the variations in entropy generations and entropy generation ratio with Reynolds number at different pitch ratios. At a given pitch ratio, the entropy generation from the heat transfer irreversibility (S_{gen}^H) decreases with increasing Reynolds number and becomes increasingly gentle, while that from the fluid friction irreversibility (S_{gen}^F) shows the opposite trend, implying that the total entropy generation (S_{gen}) decreases first and then increases with increasing Reynolds number. In other words, the irreversibility from the heat transfer dominates the source of irreversibility at low Reynolds numbers. In addition, as the Reynolds number increases, the heat transfer irreversibility reduces, while the

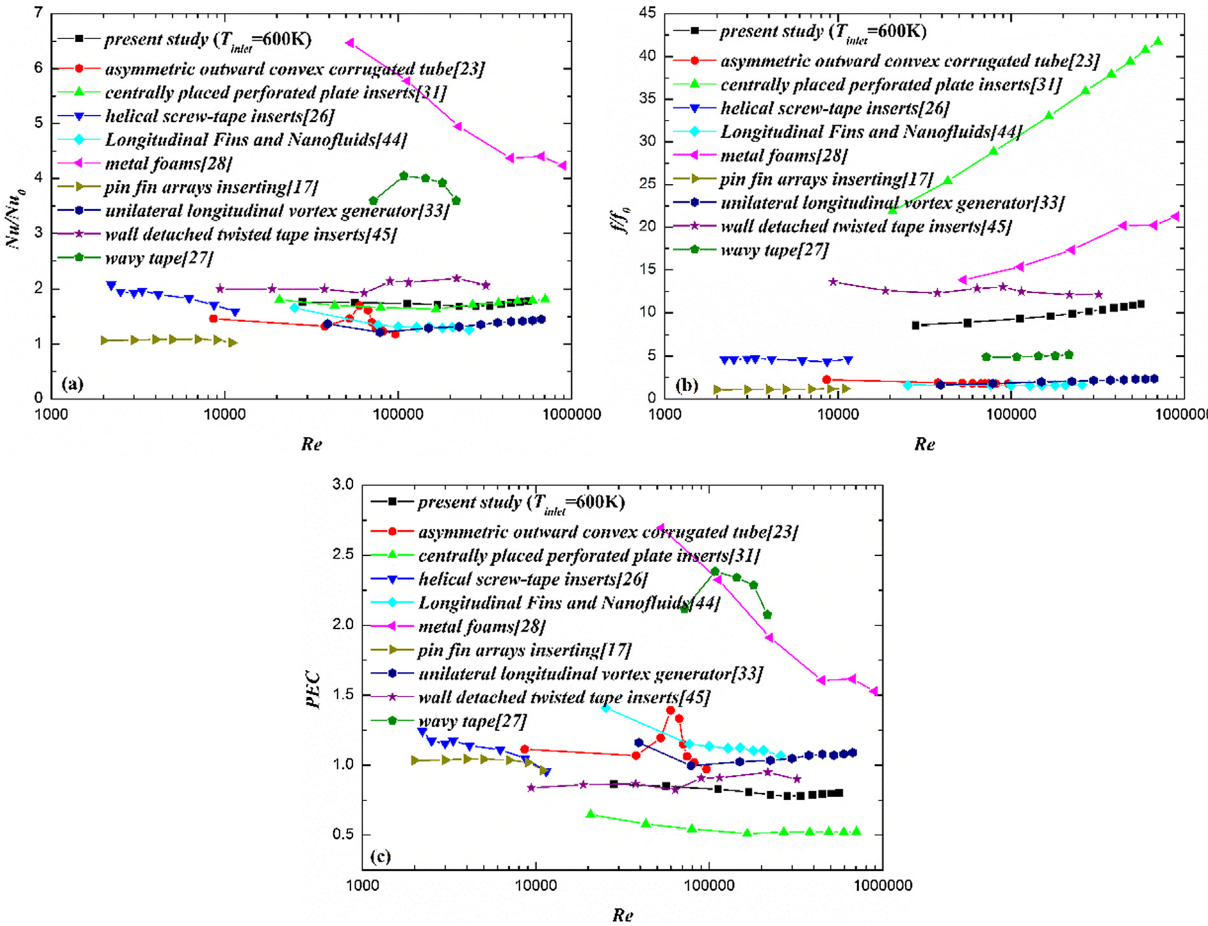

Fig. 18. Comparisons with other studies. (a) Nusselt number ratio; (b) friction factor ratio; (c) *PEC* values.

fluid friction irreversibility increases rapidly and eventually dominates the source of irreversibility. At a given Reynolds number, ${S_{gen}}^H$ decreases with a decreasing pitch ratio and is apparently lower than that of the smooth PTR, while ${S_{gen}}^F$ increases rapidly with a decreasing pitch ratio and is much higher than that of the smooth PTR. As a result, S_{gen} decreases with the decreasing pitch ratio at a low Reynolds number, and shows an opposite trend at high Reynolds numbers. The entropy generation ratio ($N_{S,en}$) shows a similar regularity to total entropy generation, and is lower than 1.

Fig. 16 shows the variations in entropy generation and entropy generation ratio with mass flow rate at different fluid inlet temperatures at d = 20 mm, β = 40°, and p^* = 2. At a given mass flow rate, ${S_{gen}}^H$ decreases with the fluid inlet temperature and all of them are clearly lower than those of the corresponding smooth PTR, while the deviations in ${S_{gen}}^F$ among different fluid inlet temperatures are limited and all of them are much higher than those of the corresponding smooth PTR, especially at high mass flow rates. The total entropy generation decreases first and then increases with the mass flow rate. Thus, the entropy generation ratio shows the same trend. Furthermore, at a given fluid inlet temperature, there is a mass flow rate (8.4 kg/s for T_{inlet} = 650 K, 9.5 kg/s for T_{inlet} = 600 K, 10.8 kg/s for T_{inlet} = 500 K and more than 12 kg/s for T_{inlet} = 400 K) beyond which $N_{S,en}$ increases beyond 1. Therefore, the mass flow rate in this study should be less than these values to ensure that the entropy generation of the enhanced PTR is lower than that of the smooth PTR. The maximum reduction in the entropy generation rate achieved in this study is approximately 74.2%.

Exergetic analysis referred to Bellos's work [12] has been conducted. The variations of exergetic efficiencies with Reynolds number and mass flow rate under different parameters are displayed in Fig. 17. It is observed that the enhanced PTRs achieve prominent enhancement in exergetic efficiency at low Reynolds number or mass flow rate but suffer exergetic efficiency loss at high Reynolds number or mass flow rate, compared to the smooth PTR. It is because the pressure drop of enhanced PTRs increase dramatically and dominate the impact on exergetic efficiency at high Reynolds number or mass flow rate. In addition, the exergetic efficiency decreases with the increase of pitch ratio at low Reynolds number while has the opposite trend at high Reynolds number. Moreover, the exergetic efficiency increases with the increase of fluid inlet temperature. The maximum enhancement in the exergetic efficiency achieved in this study is approximately 5.7%.

5.6. Limitations and comparisons with other studies

According to the professional and instructive suggestion from one of the reviewers, there are three limitations of this study. The first one is that the velocity over 1 m/s may be unrealistic and too high to be applied to practical applications. The second one is that the emissivity of the glass inner surface is set to one, which is inconsistent with the actual situation and may induce errors in the simulated results. However, the effect of the emissivity value on the simulated results has been tested, and it is found that the effect is limited and negligible. The last limitation is that the simplification of the periodic module may induce some deviations in the results between the computational domain and the total system. Generally, the thermal efficiency is expected to reduce with the increase of fluid inlet temperature or fluid temperature. In other words, the thermal efficiency is expected to decrease along the absorber tube as the fluid temperature increases along the tube. Thus, the problem of solving a small periodic part is that the thermal efficiency of the computational domain should be little higher than that of the total system under the condition of the same inlet temperature.

However, from the results in present work, the efficiency decreases slowly with the increase of the inlet temperature, for instance, the efficiency falls from 72.69% to 72.07% when the inlet temperature rises from 400 K to 500 K. In addition, the rise of fluid temperature in a full-length absorber tube in total system is about 20 °C. Therefore, the deviations induced by the simplification in the present work are considered to be small enough and acceptable.

Comparisons with previous published studies, such as those on corrugated tube [23], internally finned tubes (pin-finned tube [17], rib-finned tube [32], and longitudinal finned tube [44]), and tubes with inserts (helical screw-tape [26], wavy-tape [27], metal foams [28], centrally placed perforated plate [31], and wall detached twisted tape [45]), are presented in Fig. 18. It is observed that the absorber tube with conical strip inserts has moderate enhancements in the heat transfer and friction factor, compared to other studies. However, the *PEC* values of the PTR with conical strip inserts are lower than most other studies except the centrally placed perforated plate.

6. Conclusions

A numerical study was conducted to investigate the performances (thermal, flow, temperature and heat loss) of a PTR with conical strip inserts.

The conical strip inserts guide the cold fluid in the core region to impinge on the high-heat flux area of the absorber tube inner wall to take away the heat from the tube wall quickly. As a result, prominent reductions in the absorber tube peak temperatures and temperature gradients are obtained, especially at low Reynolds number or mass flow rate. The peak temperatures and temperature gradients are reduced by 9–230 K and 7–219 K, respectively. Consequently, the heat loss is significantly reduced, especially at low Reynolds number or mass flow rate. The maximum reduction in heat loss is 82.1%, and they are all dependent on the geometric parameters of the inserts, fluid inlet temperature, and Reynolds number or mass flow rate.

The geometric parameters of the inserts, fluid inlet temperature, and Reynolds number or mass flow rate strongly impact on the heat transfer and flow resistance. For all geometric parameters of the inserts, the fluid inlet temperatures and Reynolds numbers or mass flow rates considered, the Nusselt number is enhanced by 45–203%, while the friction factor is 6.17–17.44 times that of the smooth PTR. Consequently, the overall thermal-hydraulic performance (*PEC*) ranges from 0.70 to1.33. The thermal efficiency is enhanced by 0.02–5.04%.

From the entropy analysis, it is found that the conical strip inserts can improve the thermodynamic performance of PTR by effectively reducing the entropy generation rate. The maximum reduction in the entropy generation rate achieved in this study is 74.2%. Moreover, ${S_{gen}}^H$ decreases with the increasing Reynolds number or mass flow rate and becomes more and more gradual, while ${S_{gen}}^F$ shows opposite trends, where S_{gen} and $N_{S,en}$ decrease first and then increase with the increasing Reynolds number or mass flow rate. At the given values of geometric parameters and fluid inlet temperature, there is a Reynolds number or mass flow rate below which the entropy generation rate is lower than that of the smooth PTR. The enhanced PTRs achieve prominent enhancement in exergetic efficiency at low Reynolds number or mass flow rate but suffer exergetic efficiency loss at high Reynolds number or mass flow rate, compared to the smooth PTR. The maximum enhancement in the exergetic efficiency is approximately 5.7%.

Acknowledgment

The work was supported by the National Natural Science Foundation of China (Grant No. 51736004), the National Natural Science Foundation of China (51376069) and the National Natural Science Foundation of China Youth Project (51606073).

References

[1] Kumaresan G, Sudhakar P, Santosh R, Velraj R. Experimental and numerical studies of thermal performance enhancement in the receiver part of solar parabolic trough collectors. Renew Sustain Energy Rev 2017;77:1363–74.

[2] Hafez AZ, Attia AM, Eltwab HS, ElKousy AO, Afifi AA, AbdElhamid AG, et al. Design analysis of solar parabolic trough thermal collectors. Renew Sustain Energy Rev 2018;82:1215–60.

[3] Yang S, Sensoy TS, Ordonez JC. Dynamic 3D volume element model of a parabolic trough solar collector for simulation and optimization. Appl Energy 2018;217:509–26.

[4] Sandeep HM, Arunachala UC. Solar parabolic trough collectors: a review on heat transfer augmentation techniques. Renew Sustain Energy Rev 2017;69:1218–31.

[5] Mwesigye A, Bello-Ochende T, Meyer JP. Numerical investigation of entropy generation in a parabolic trough receiver at different concentration ratios. Energy 2013;53:114–27.

[6] Bellos E, Tzivanidis C, Tsimpoukis D. Enhancing the performance of parabolic trough collectors using nanofluids and turbulators. Renew Sustain Energy Rev 2018;91:358–75.

[7] Fuqiang W, Ziming C, Jianyu T, Yuan Y, Yong S, Linhua L. Progress in concentrated solar power technology with parabolic trough collector system: a comprehensive review. Renew Sustain Energy Rev 2017;79:1314–28.

[8] Verma SK, Tiwari AK. Progress of nanofluid application in solar collectors: a review. Energy Convers Manage 2015;100:324–46.

[9] Mwesigye A, Meyer JP. Optimal thermal and thermodynamic performance of a solar parabolic trough receiver with different nanofluids and at different concentration ratios. Appl Energy 2017;193:393–413.

[10] Mwesigye A, Huan Z, Meyer JP. Thermal performance and entropy generation analysis of a high concentration ratio parabolic trough solar collector with Cu-Therminol®VP-1 nanofluid. Energy Convers Manage 2016;120:449–65.

[11] Kasaeian A, Daviran S, Azarian RD, Rashidi A. Performance evaluation and nanofluid using capability study of a solar parabolic trough collector. Energy Convers Manage 2015;89:368–75.

[12] Bellos E, Tzivanidis C, Tsimpoukis D. Thermal, hydraulic and exergetic evaluation of a parabolic trough collector operating with thermal oil and molten salt based nanofluids. Energy Convers Manage 2018;156:388–402.

[13] Toghyani S, Baniasadi E, Afshari E. Thermodynamic analysis and optimization of an integrated Rankine power cycle and nano-fluid based parabolic trough solar collector. Energy Convers Manage 2016;121:93–104.

[14] Coccia G, Di Nicola G, Colla L, Fedele L, Scattolini M. Adoption of nanofluids in low-enthalpy parabolic trough solar collectors: Numerical simulation of the yearly yield. Energy Convers Manage 2016;118:306–19.

[15] Subramani J, Nagarajan PK, Mahian O, Sathyamurthy R. Efficiency and heat transfer improvements in a parabolic trough solar collector using TiO2 nanofluids under turbulent flow regime. Renew Energy 2018;119:19–31.

[16] Gupta M, Singh V, Kumar R, Said Z. A review on thermophysical properties of nanofluids and heat transfer applications. Renew Sustain Energy Rev 2017;74:638–70.

[17] Gong X, Wang F, Wang H, Tan J, Lai Q, Han H. Heat transfer enhancement analysis of tube receiver for parabolic trough solar collector with pin fin arrays inserting. Sol Energy 2017;144:185–202.

[18] Bellos E, Tzivanidis C, Tsimpoukis D. Optimum number of internal fins in parabolic trough collectors. Appl Therm Eng 2018;137:669–77.

[19] Muñoz J, Abánades A. Analysis of internal helically finned tubes for parabolic trough design by CFD tools. Appl Energy 2011;88:4139–49.

[20] Bellos E, Tzivanidis C, Daniil I, Antonopoulos KA. The impact of internal longitudinal fins in parabolic trough collectors operating with gases. Energy Convers Manage 2017;135:35–54.

[21] Huang Z, Li Z-Y, Yu G-L, Tao W-Q. Numerical investigations on fully-developed mixed turbulent convection in dimpled parabolic trough receiver tubes. Appl Therm Eng 2017;114:1287–99.

[22] Fuqiang W, Qingzhi L, Huaizhi H, Jianyu T. Parabolic trough receiver with corrugated tube for improving heat transfer and thermal deformation characteristics. Appl Energy 2016;164:411–24.

[23] Fuqiang W, Zhexiang T, Xiangtao G, Jianyu T, Huaizhi H, Bingxi L. Heat transfer performance enhancement and thermal strain restrain of tube receiver for parabolic trough solar collector by using asymmetric outward convex corrugated tube. Energy 2016;114:275–92.

[24] Bitam EW, Demagh Y, Hachicha AA, Benmoussa H, Kabar Y. Numerical investigation of a novel sinusoidal tube receiver for parabolic trough technology. Appl Energy 2018;218:494–510.

[25] Mwesigye A, Bello-Ochende T, Meyer JP. Heat transfer and entropy generation in a parabolic trough receiver with wall-detached twisted tape inserts. Int J Therm Sci 2016;99:238–57.

[26] Song X, Dong G, Gao F, Diao X, Zheng L, Zhou F. A numerical study of parabolic trough receiver with nonuniform heat flux and helical screw-tape inserts. Energy 2014;77:771–82.

[27] Zhu X, Zhu L, Zhao J. Wavy-tape insert designed for managing highly concentrated solar energy on absorber tube of parabolic trough receiver. Energy 2017;141:1146–55.

[28] Wang P, Liu DY, Xu C. Numerical study of heat transfer enhancement in the receiver tube of direct steam generation with parabolic trough by inserting metal foams. Appl Energy 2013;102:449–60.

[29] Jamal-Abad MT, Saedodin S, Aminy M. Experimental investigation on a solar parabolic trough collector for absorber tube filled with porous media. Renew

Energy 2017;107:156–63.
[30] Ravi Kumar K, Reddy KS. Thermal analysis of solar parabolic trough with porous disc receiver. Appl Energy 2009;86:1804–12.
[31] Mwesigye A, Bello-Ochende T, Meyer JP. Heat transfer and thermodynamic performance of a parabolic trough receiver with centrally placed perforated plate inserts. Appl Energy 2014;136:989–1003.
[32] Cheng ZD, He YL, Cui FQ. Numerical study of heat transfer enhancement by unilateral longitudinal vortex generators inside parabolic trough solar receivers. Int J Heat Mass Transf 2012;55:5631–41.
[33] Liu W, Liu P, Wang JB, Zheng NB, Liu ZC. Exergy destruction minimization: A principle to convective heat transfer enhancement. Int J Heat Mass Transf 2018;122:11–21.
[34] Liu P, Zheng N, Shan F, Liu Z, Liu W. An experimental and numerical study on the laminar heat transfer and flow characteristics of a circular tube fitted with multiple conical strips inserts. Int J Heat Mass Transf 2018;117:691–709.
[35] Shih T-H, Liou WW, Shabbir A, Yang Z, Zhu J. A new k-ϵ eddy viscosity model for high reynolds number turbulent flows. Comput Fluids 1995;24:227–38.
[36] Fluent Incorporated, User's Guide for FLUENT/UNS and RAMPANT, Release 4.0, vol. 1, 2, and 4, Fluent Incorporated, Lebanon. NH 03766, USA; 1996.
[37] Mwesigye A, Bello-Ochende T, Meyer JP. Minimum entropy generation due to heat transfer and fluid friction in a parabolic trough receiver with non-uniform heat flux at different rim angles and concentration ratios. Energy 2014;73:606–17.
[38] Forristall R. Heat transfer analysis and modeling of a parabolic trough solar receiver implemented in engineering equation solver. Technical, Report, NREL/TP-550-34169; 2003.
[39] Mullick SC, Nanda SK. An improved technique for computing the heat loss factor of a tubular absorber. Sol Energy 1989;42:1–7.
[40] Webb R. Performance evaluation criteria for use of enhanced heat transfer surfaces in heat exchanger design. Int J Heat Mass Transf 1981;24:715–26.
[41] Deshmukh PW, Vedula RP. Heat transfer and friction factor characteristics of turbulent flow through a circular tube fitted with vortex generator inserts. Int J Heat Mass Transf 2014;79:551–60.
[42] SM. Dudley EV; Kolb JG, Kearney D. SEGS LS2 solar collector-test results. Report of Sandia National Laboratories; 1994, SAN94-1884.
[43] He Y-L, Xiao J, Cheng Z-D, Tao Y-B. A MCRT and FVM coupled simulation method for energy conversion process in parabolic trough solar collector. Renew Energy 2011;36:976–85.
[44] Amina B, Miloud A, Samir L, Abdelylah B, Solano JP. Heat transfer enhancement in a parabolic trough solar receiver using longitudinal fins and nanofluids. J Therm Sci 2016;25:410–7.
[45] Mwesigye A, Bello-Ochende T, Meyer JP. Heat transfer enhancement in a parabolic trough receiver using wall detached twisted tape inserts; 2013, V06BT7A03.